Supplemental Information

Supplementary Figures

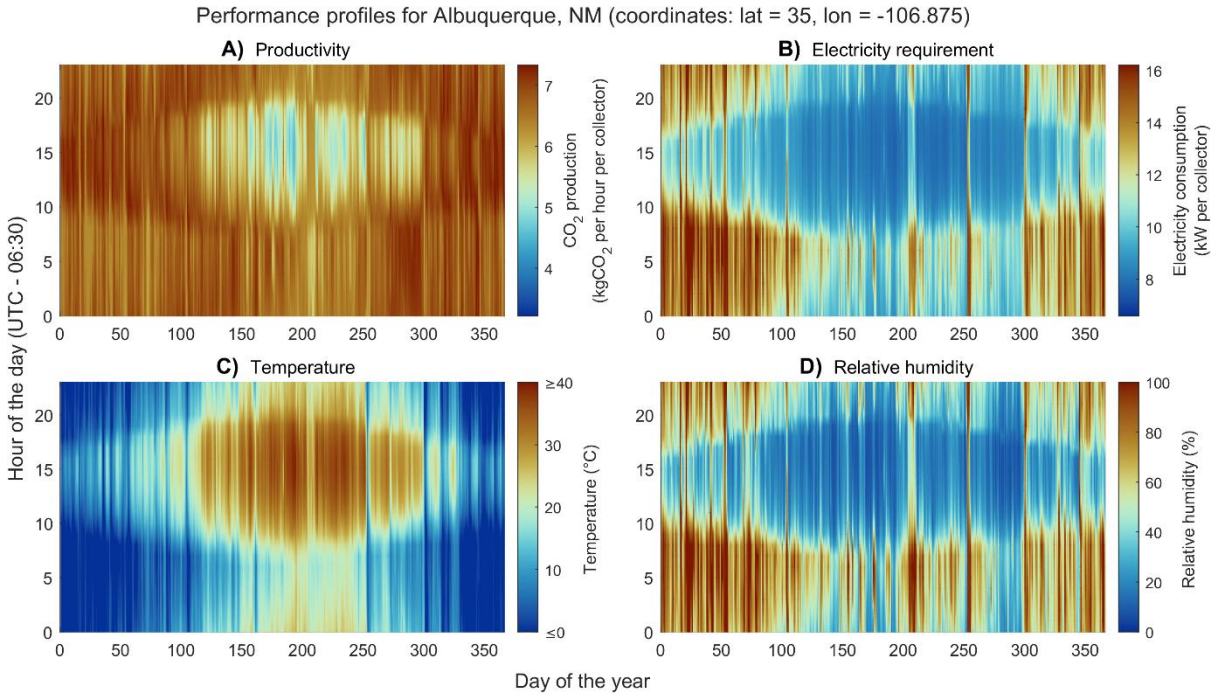

Figure S1. Hourly DAC performance and ambient condition for Albuquerque, NW (cold dry climate) using 2020 data. Hourly production and electricity consumption assume steady production equivalent to a large scale plant where process cycles for different collectors are synchronized.

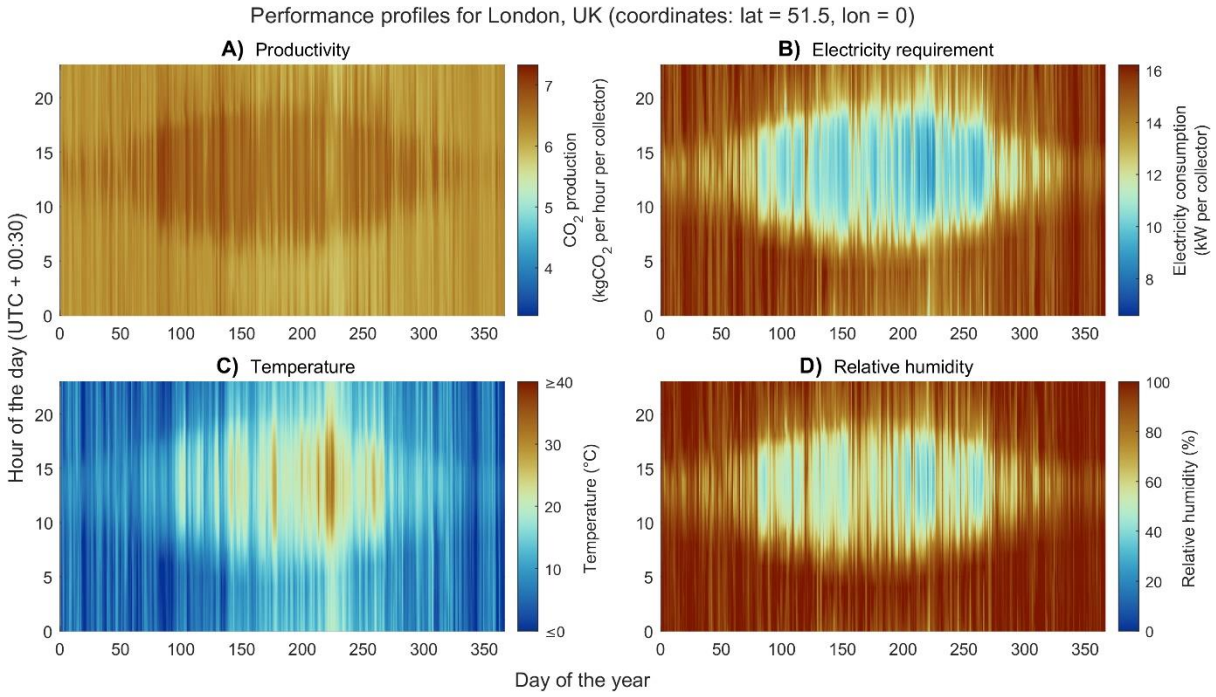

Figure S2. Hourly DAC performance and ambient condition for London, UK (cold humid climate) using 2020 data. Hourly production and electricity consumption assume steady production equivalent to a large scale plant where process cycles for different collectors are synchronized.

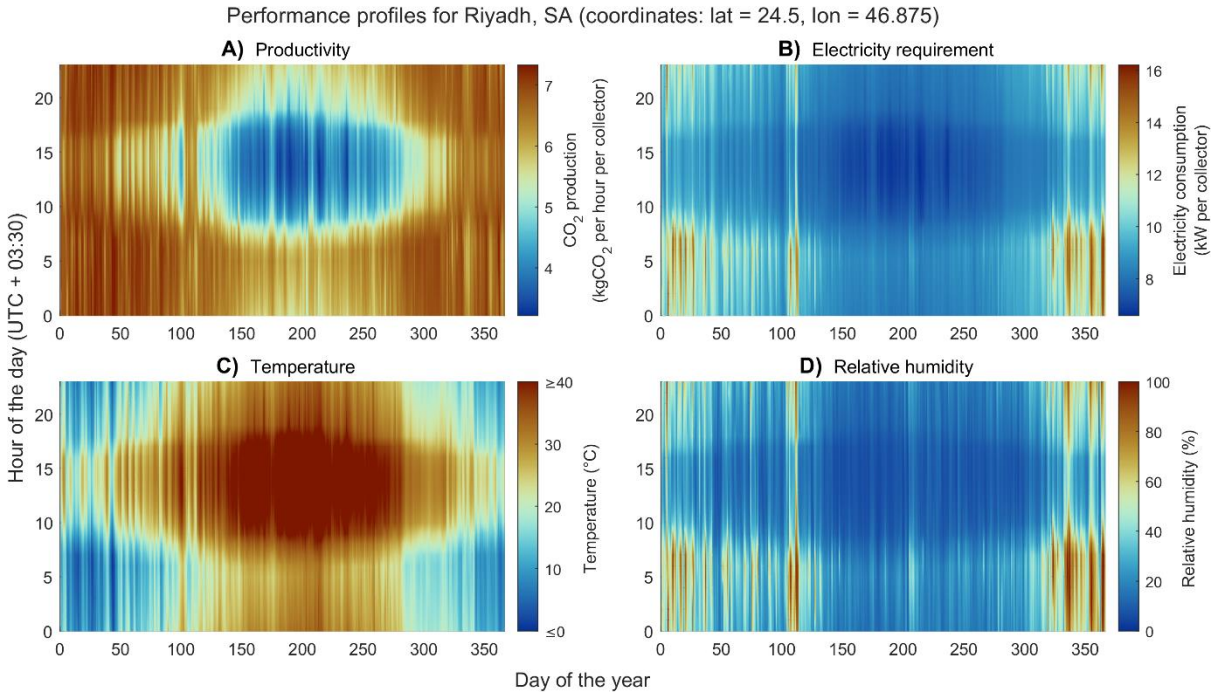

Figure S3. Hourly DAC performance and ambient condition for Riyadh, SA (Hot dry climate) using 2020 data. Hourly production and electricity consumption assume steady production equivalent to a large scale plant where process cycles for different collectors are synchronized.

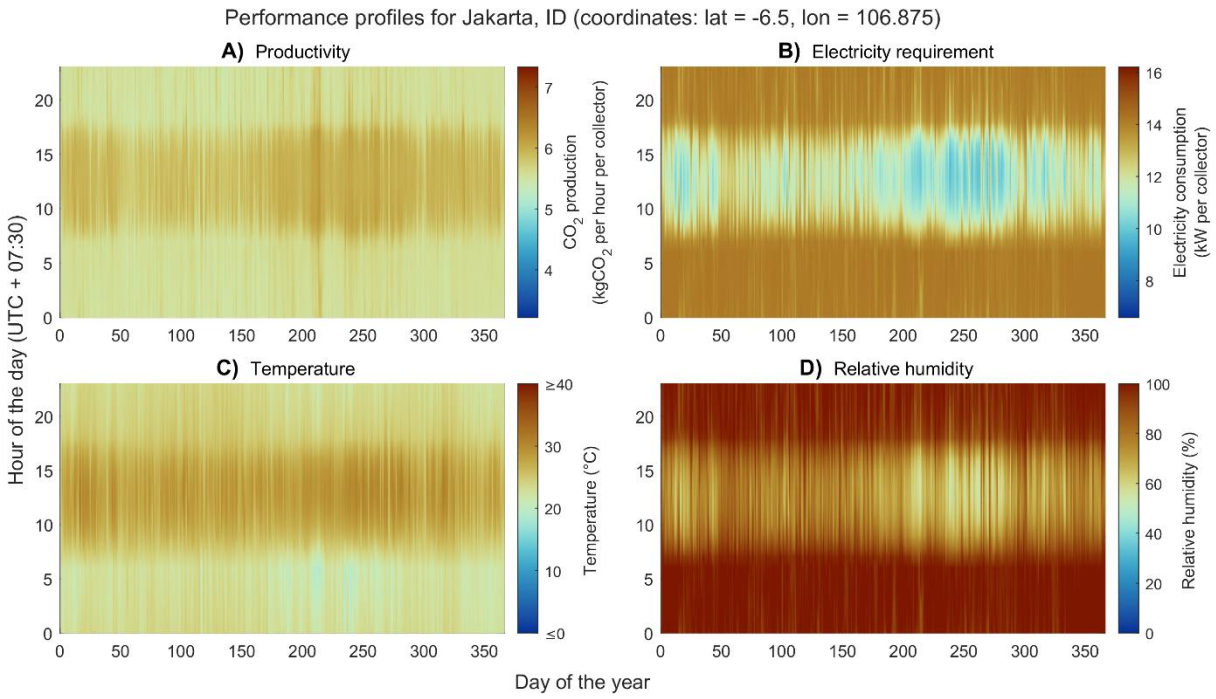

Figure S4. Hourly DAC performance and ambient condition for Jakarta, ID (Hot humid climate) using 2020 data. Hourly production and electricity consumption assume steady production equivalent to a large scale plant where process cycles for different collectors are synchronized.

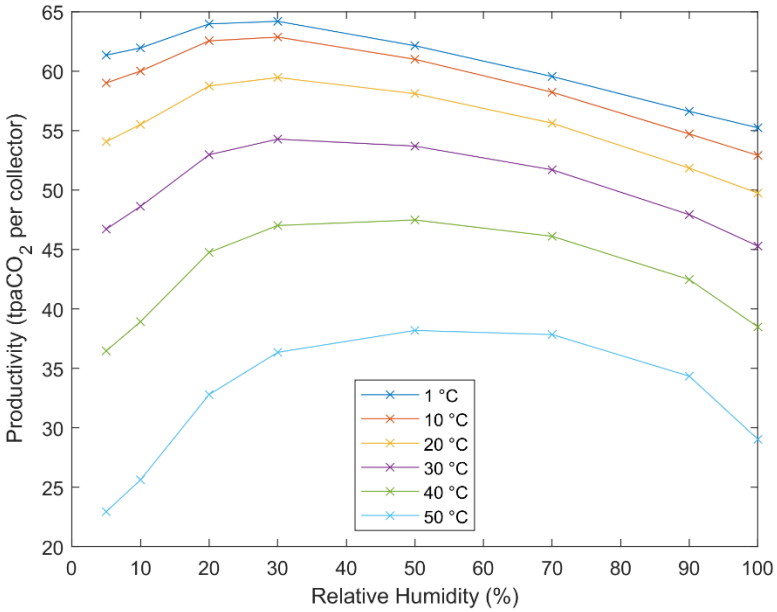

Figure S5. Effect of relative humidity and temperature on productivity ($tpaCO_2$ per collector). It can be seen that both temperature and relative humidity have an observable effect on process productivity.

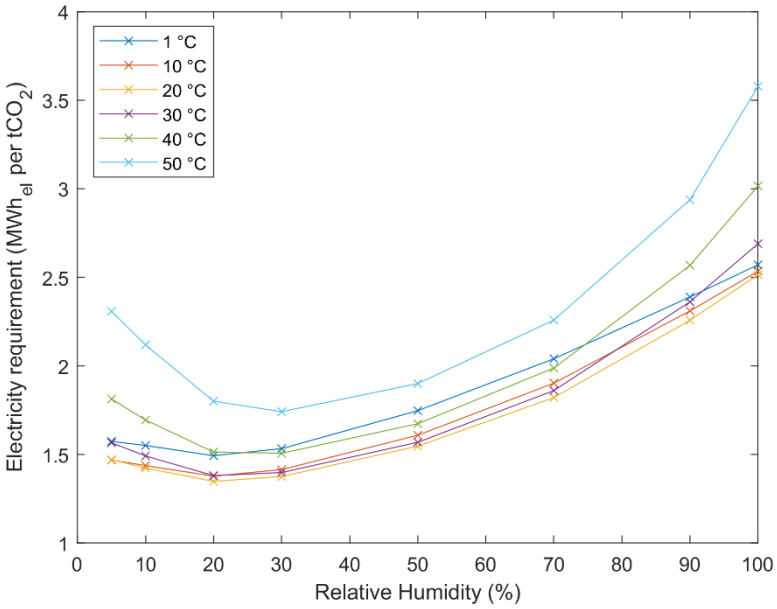

Figure S6. Effect of relative humidity and temperature on electricity requirement (MWh_{el} per tCO_2). It can be seen that relative humidity has a more pronounced effect (than temperature) on the total electricity requirement.

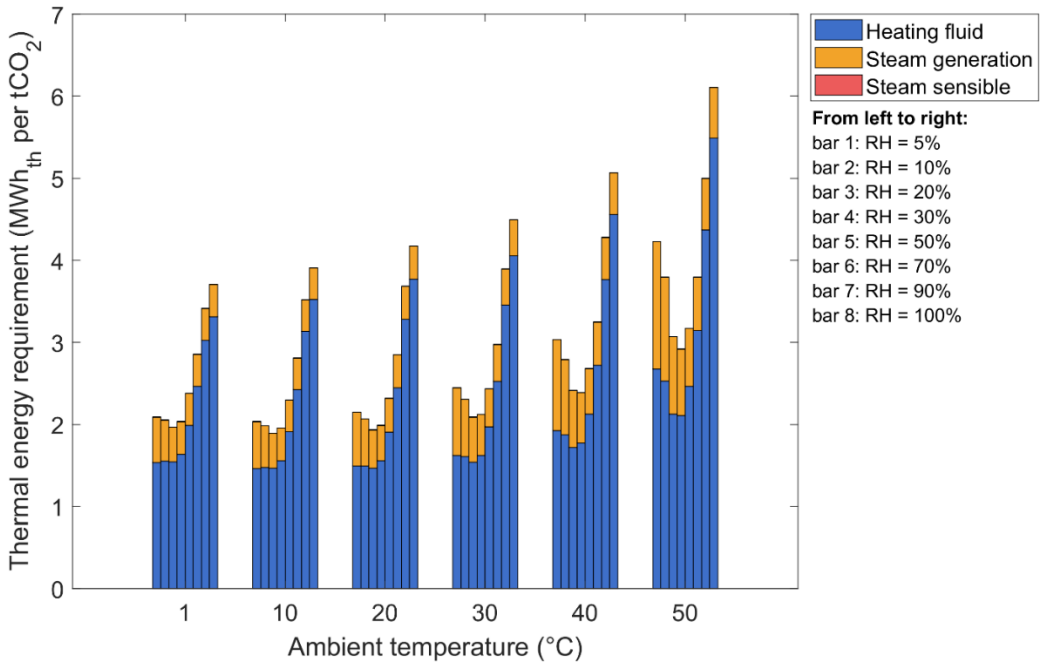

Figure S7. Thermal energy requirement breakdown. The thermal energy requirement for preheating the steam water supply is zero for all conditions as this heat requirement is met by the recovered heat from compressing the process gasses (Experimental Procedures).

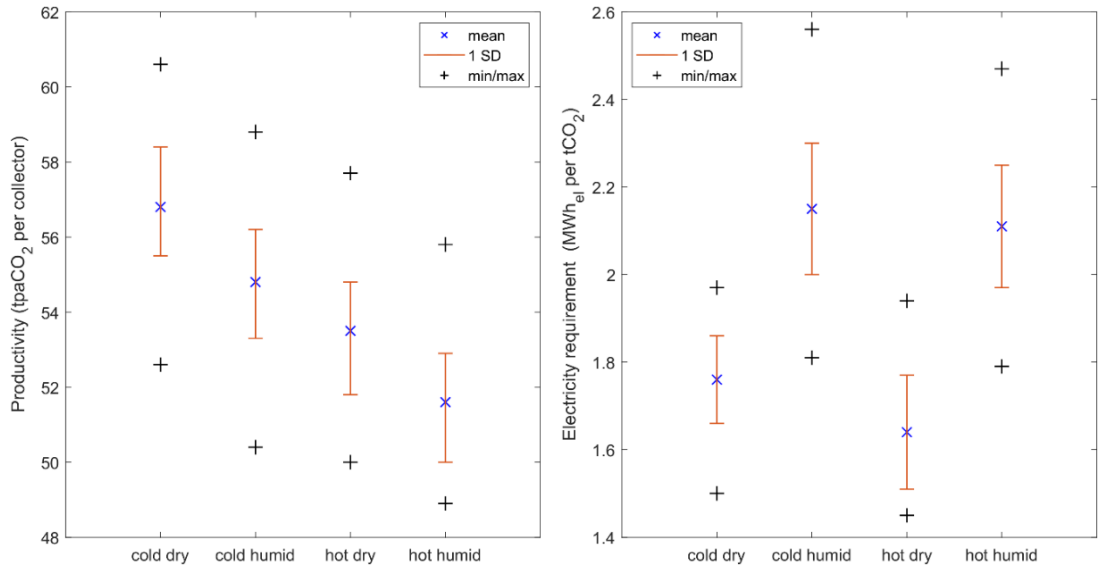

Figure S8. Global DAC performance data visualization. The variation in DAC performance is mainly due to the effect of regional climate. SD is standard deviation. Please find details about the calculation of standard deviation in Note S.7

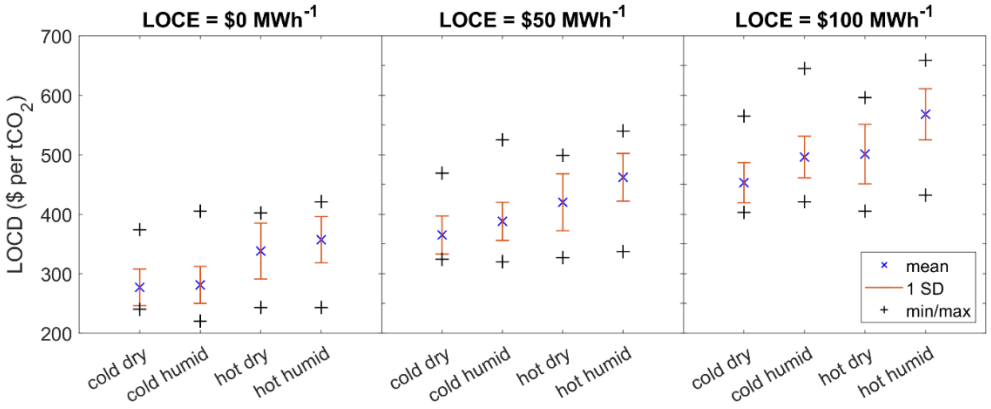

Figure S9. LCOD at different climates conditions and LCOEs. The variation in LCOD is due to the variation of regional DAC performance (due to the variation in regional climate) and WACC. SD is the standard deviation. Please find details about the calculation of standard deviation in Note S.7.

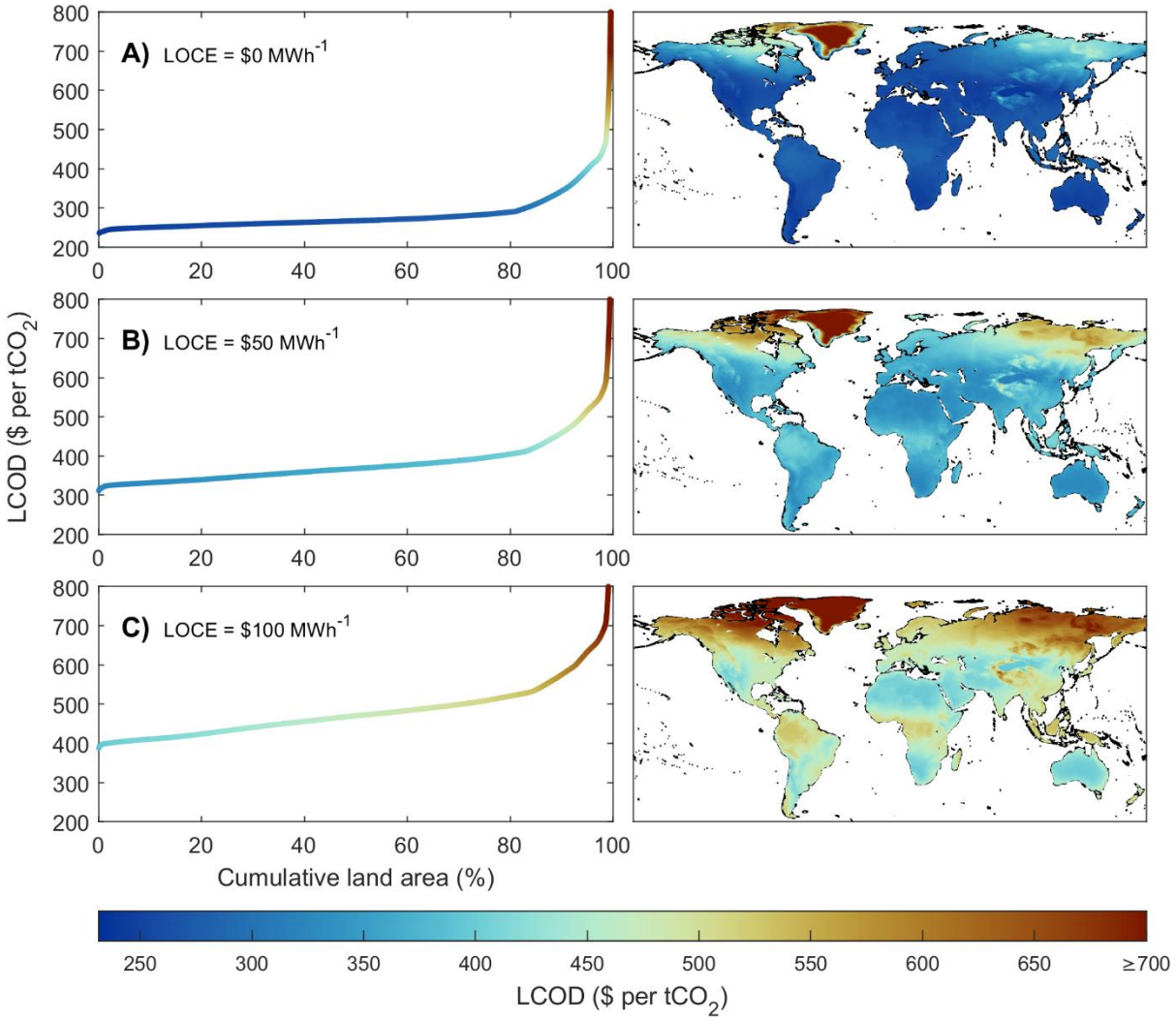

59

60 **Figure S10. Global DAC supply curves at different LOCEs when WACC is fixed at 5%.** Here, the
61 variation in LCOD is mainly due to the variation of DAC performance affected by regional climate.

62

Supplementary Tables

Table S1. Economic analysis assumptions.

	Purchased cost[a]		Lifetime (years)	Source
CO_2 collector	20,000	$ per collector	25	[b]Based on a mid-sized car
Fan	0.89[c]	$ per (m^3/h)	25	[1]
Vacuum pump, Compressor, and heat pumps[d]	312,547	$ per MW_{el}	25	[1]
Sorbent	2,000	$ per ton sorbent	4	[2]

[a] All costs are adjusted to 2020 using CE index = 596.2.

[b] The CO_2 collector cost can be estimated based on the similarity of the materials used to manufacture it compared to cars[3,4], including steel, aluminium, plastics, insulation, etc. Similar to a car, the CO_2 collector is modular; therefore, it can be manufactured using similar process methods used for car manufacturing. Moreover, a material assessment of the CO_2 collector can estimate the amount of materials needed for each collector. Each collector has 6 square-shaped steel walls, two of which are movable, with each side having dimensions of around 1.45 m. Assuming a wall thickness of 0.01 m, the total steel weight needed is 990 kg at a density of 7850 kg per m^3. Each collector has 88 frames. Each frame consists of 21.3 m of aluminium tubes with a diameter of 0.01 m and a thickness of 0.001 m. Thus, each collector contains 242 kg of aluminium tubes at a density of 2710 kg per m^3. Aluminium mesh is used to improve the bed thermal conductivity where each frame contains 1.9 kg of aluminium mesh based on the ratio used in Climeworks patent[3], resulting in an additional 166.5 kg of aluminium per collector. Additional aluminium and plastic are used for C-profiles, sturts, wedge spacers and sealing strips at a ratio of 0.53 kg per frame or 46.5 kg per collector. Based on this calculation, the material needed for one collector is around 1446 kg per collector, including steel, aluminium and plastic. This can be compared to a mid-sized car's average weight of around 1500 kg (ref[5]).

[c] CAPEX (Experimental Procedures).

[d] Heat pumps are estimated based on the main process equipment (compressors) cost, then adjusted to account for the total installed cost, including auxiliary equipment using Lang Factor (Experimental Procedures).

Note S1: adsorption model parameters

The table below summarizes the model parameters used for the adsorption model.

Adsorption model parameters.

	Symbol	Value	Unit	Source
Bed				
Width of the sorbent bed	b	1.43	m	
Height of the sorbent bed	h	0.1	m	
Length of the sorbent bed	l	1.72×10^{-2}	m	
Solid density	ρ_s	812.2	kg m^{-3}	[6]
Envelope density	ρ_e	635.2	kg m^{-3}	[7]
Bulk density	ρ_b	356.4	kg m^{-3}	Calculated
Internal porosity	ε_P	0.22		Calculated
Total porosity	ε_t	0.56		Calculated
Particle size	d_P	7.5×10^{-4}	m	[7]
Thermal conductivity of sorbent and bed	k_{eff}	0.16 × 3.6	W m^{-1} K^{-1}	Estimated from[3,8]
Heat capacity of sorbent and bed	Cp_s	1.5 + 0.38	kJ kg^{-1} K^{-1}	Sorbent[6] bed[3]
Feed				
Feed gas velocity	u_{feed}	0.028	m s^{-1}	
CO_2				
Heat capacity of adsorbed CO_2	$Cp_{CO_2,ads}$	2.0	kJ kg^{-1} K^{-1}	[8]
Heat capacity of $CO_{2(g)}$	$Cp_{CO_2,g}$	0.86	kJ kg^{-1} K^{-1}	[8]
Heat of adsorption of CO_2	$\Delta h_{ads,CO_2}$	70	kJ mol^{-1}	[7]
Mass transfer coefficient of CO_2	k_{CO_2}	3×10^{-3}	s^{-1}	[7]
Specific volume of adsorbed CO_2	$v_{CO2,ads}$	1×10^{-3}	m^3 kg^{-1}	[8]
Molecular weight of CO_2	MW_{CO2}	44×10^{-3}	kg mol^{-1}	
Concentration of CO_2	y_{CO2}	400	ppm	
H_2O				
Heat capacity of adsorbed H_2O	$Cp_{H_2O,ads}$	4.19	kJ kg^{-1} K^{-1}	[8]
Heat capacity of $H_2O_{(g)}$	$Cp_{H_2O,g}$	1.9	kJ kg^{-1} K^{-1}	[8]
Heat of adsorption of H_2O	$\Delta h_{ads,H_2O}$	46	kJ mol^{-1}	[7]
Mass transfer coefficient of H_2O	k_{H_2O}	8.6×10^{-3}	s^{-1}	[7]
Specific volume of adsorbed H_2O	$v_{H2O,ads}$	1×10^{-3}	m^3 kg^{-1}	[8]
Molecular weight of H_2O	MW_{H2O}	18×10^{-3}	kg mol^{-1}	
Concentration of H_2O	y_{H2O}	[a]	mol H_2O mol^{-1}	
Air (mostly N_2 and O_2)				
Heat capacity of $air_{(g)}$	$Cp_{air,g}$	1.01	kJ kg^{-1} K^{-1}	[8]
Molecular weight of air	MW_{air}	28.97×10^{-3}	kg mol^{-1}	
Concentration of air	y_{air}	[b]	mol air mol^{-1}	
Diffusion				
Average diffusion coefficient	D_0	2.2×10^{-5}	m^2 s^{-1}	[8]

[a]The concentration of H_2O varies based on the relative humidity.

[b]The concentration of air varies based on the concentration of H_2O which calculated as $1 - y_{CO2} - y_{H2O}$

The following are some comments regarding the model parameters.

- The reported sorbent envelope density is 630–710 kg m^{-3} (Young el al.[7]). 635.2 kg m^{-3} is used here as the envelope density to simplify the analysis. At this envelope density, each CO_2 collector contains 1000 kg of sorbent. Solid density (ρ_s), envelope density (ρ_e), and bulk density (ρ_b) are defined in Equations 1–3 where V_T, V_X, V_P, and M are total system volume, external void volume, internal void volume (pore volume), and mass.

$$\rho_s = \frac{M_{particles}}{V_T - V_X - V_P} \quad (1)$$

$$\rho_e = \frac{M_{particles}}{V_T - V_X} \quad (2)$$

$$\rho_b = \frac{M_{particles}}{V_T} \quad (3)$$

- When calculating the bed porosity, it was assumed that the aluminium mesh occupies around 3.8% of the sorbent cell, based on an estimate from the patent[3].
- The reported particle diameter for the modelled sorbent is in the range of 3.15×10^{-4} – 1.25×10^{-3} m (Young el al.[7]). 7.5×10^{-4} m is used, which is around the average, as at this particle diameter, the pressure drop for 1×10^{-2} m thickness bed is around 1 mbar when air velocity is 0.028 m s^{-1}. This pressure drop at this air velocity is aligned with the data presented in the patent[3].
- The thermal conductivity of the sorbent bed was estimated from the patent testing [3]. In the testing, a sorbent cell similar to the one modelled here was heated by flowing a heating fluid through the heating tube with a temperature of 93.6 °C, with the centre of the bed reaching a temperature of 85 °C after 90 minutes. Process condition information such as the sorbent condition and desorption pressure for the testing was not reported in the patent. It was assumed here that the sorbent was saturated with CO_2 and H_2O under an ambient condition of 20°C and RH of 40%. Two desorption pressures were used to estimate the thermal conductivity: 1000 mbar and 100 mbar. The figure below shows the model fit on the patent testing data and the estimated thermal conductivity for the two desorption pressures which is in the range of 0.42–0.72 W m^{-1} K^{-1} . It was not possible to obtain an exact fit, mainly due to the missing process information from the patent. However, in both fits, the bed centre temperature reached around 85 °C within 90 minutes. The sorbent used in the patent was amine-functionalized cellulose which has a thermal conductivity of 44.5×10^{-3} W m^{-1} k^{-1} [8]. Considering the calculated thermal conductivity (0.42−0.72 W m^{-1} K^{-1}), this corresponds to an improvement between 9−16 times the thermal conductivity of cellulose by incorporating the aluminium mesh design, which is probably reasonable given that aluminium thermal conductivity is 205 W m^{-1} K^{-1}. For Lewatit VP OC 1065, the thermal conductivity is 0.16 W m^{-1} K^{-1} (Young el al.[7]). It is assumed that the thermal conductivity of the modelled bed using Lewatit VP OC 1065 is the average of the fitted range, which is 0.57 W m^{-1} K^{-1}. This implies that the thermal conductivity of the bed did not improve when Lewatit VP OC 1065, with better thermal conductivity, was used instead of the cellulose sorbent. Also, thermal conductivity of the bed has been improved by 3.6 times compared to the Lewatit VP OC 1065 thermal conductivity when incorporating the aluminium mesh. This might be in the conservative range given that the thermal conductivity of aluminium is 3 orders of magnitude larger than Lewatit VP OC 1065.

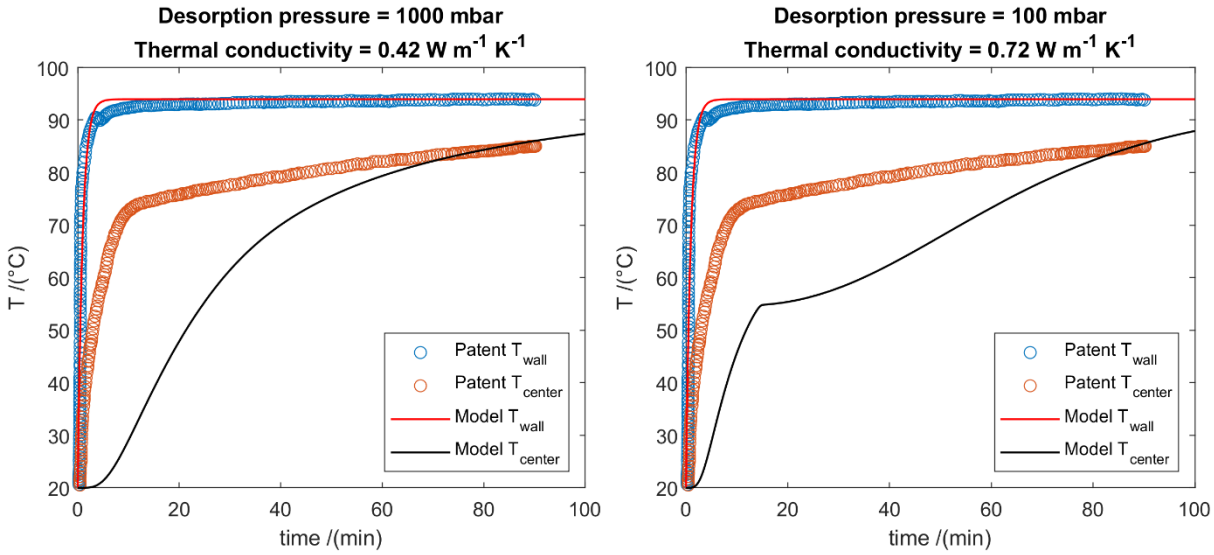

Thermal conductivity patents[3] data fitting.

- To account for the heating tubes and aluminium mesh heat capacity, 0.38 kJ kg^{-1} K^{-1} was added to the sorbent heat capacity based on the ratio used in the frame design reported in Climeworks patent[3].
- In Wurzbacher et al.[8] work, it was found that diffusion has a strong effect on the temperature profile of the process especially when operating at vacuum, as diffusion is inversely proportional to pressure. However, their simplified approach using an average value for the 3-component mixture of CO_2, water and air did not affect the accuracy of the modelling. Therefore, the same approach is adopted in this work.

Note S2: Isotherm model parameters

The following two tables show the isotherm model parameters that are used in this work which is based on Young el al.[7]

Mechanistic and WADST co-adsorption model fitting parameters[7].

Parameter	Value	Unit
T_0	298.15	K
$q_{\infty,0}$	4.86	mol kg^{-1}
$\varkappa$	0	(–)
b_0	2.85 × 10^{-21}	Pa^{-1}
$-\Delta H_0$	117,798	J mol^{-1}
τ_0	0.209	(–)
α	0.523	(–)
ϕ_{max}	1.000	(–)
$f_{blocked,max}$	0.433	(–)
k	0.795	kg mol^{-1}
ϕ_{dry}	1.000	(–)
A	1.535	mol kg^{-1}
$-\Delta H_{wet}$	130,155	J mol^{-1}
n	1.425	(–)

GAB model fitting parameters[7].

Parameter	Value	Unit
q_m	3.63	mol kg^{-1}
C	47,110	J mol^{-1}
D	0.023744	K^{-1}
F	57.706	J mol^{-1}
G	−47.814	J mol^{-1} K^{-1}

Note S3: Adsorption model boundary conditions

The boundary conditions for all simulated cyclic steps are shown in table below where N is the number of finite volume cells. $\dot{F}$, A, y_i, P and p are volumetric flow rate, cross sectional area in the flow direction, gas concentration of component I, total pressure and partial pressure, respectively. x, y and z are variables for space as shown in Figure 7. In the 1D model, $^1/_2$ represents the boundary wall of the first finite volume cell, which is equivalent to $z = 0$, and $N + {}^1/_2$ represents the boundary wall of the last finite volume cell, which is equivalent to $z = l$.

For each cyclic step, the initial conditions for the variables are the final values of the variables from the previous step. When there is a transition from the 1D model to the 2D model, the variable average over the z-axis or x-y plane in case of the 1D model or 2D model, respectively, from the previous step is used as an initial condition for the current step. k_{BL} corresponds to the valve equation controlling the pressure where a value of 0.25 s^{-1} is used. More detailed of each cyclic step and process description is presented in Note S4.

Adsorption model boundary conditions.

Step	Model	Boundary conditions	
Adsorption (Ads)	1D	**At $z_{1/2}$:** • Pressure $P_{1/2} = P_1 - \frac{1}{2}\frac{\partial P}{\partial z}_{1/2}$ • Gas velocity $u_{1/2} = \frac{\dot{F}_{feed}}{A}$ • Temperature $T_{1/2} = T_{air}$ • Concentration $y_{i\,1/2} = y_{i,air\,1/2}$, $i = CO_2, H_2O, Air$	**At $z_{N+1/2}$:** • Pressure $P_{N+1/2} = P_{ads}$ • Gas velocity $\frac{\partial u}{\partial z}_{N+1/2} = 0$ • Temperature $\frac{\partial T}{\partial z}_{N+1/2} = 0$ • Concentration $\frac{\partial y_i}{\partial z}_{N+1/2} = 0, \quad i = CO_2, H_2O, Air$
Blowdown (BL)	1D	**At $z_{1/2}$:** • Pressure $\frac{\partial P}{\partial z}_{1/2} = 0$ • Gas velocity $u_{1/2} = 0$	**At $z_{N+1/2}$:** • Pressure $\frac{\partial P}{\partial z}_{N+1/2} = k_{BL}\left(P_{Des} - P_{N+1/2}\right)$ • Gas velocity $\frac{\partial u}{\partial z}_{N+1/2} = 0$

		• Temperature $\frac{\partial T}{\partial z_{1/2}} = 0$ • Concentration $\frac{\partial y_i}{\partial z_{1/2}} = 0, \quad i = CO_2, H_2O, Air$	• Temperature $\frac{\partial T}{\partial z_{N+1/2}} = 0$ • Concentration $\frac{\partial y_i}{\partial z_{N+1/2}} = 0, \quad i = CO_2, H_2O, Air$
Desorption – bed heating (Des)	2D	**At $x = 0$ or $y = 0$** • Temperature $T(x = 0, y, t) = T_{wall}(t)$ $T(x, y = 0, t) = T_{wall}(t)$ • Concentration $\left.\frac{\partial p_i}{\partial x}\right\|_{x=0} = 0, \quad i = CO_2, H_2O, Air$ $\left.\frac{\partial p_i}{\partial y}\right\|_{y=0} = 0, \quad i = CO_2, H_2O, Air$	**At $x = \frac{b}{2}$ or $y = h$** • Temperature $\left.\frac{\partial T}{\partial x}\right\|_{x=\frac{b}{2}} = 0$ $\left.\frac{\partial T}{\partial y}\right\|_{y=h} = 0$ • Concentration $\left.\frac{\partial p_i}{\partial x}\right\|_{x=\frac{b}{2}} = 0, \quad i = CO_2, H_2O, Air$ $\left.\frac{\partial p_i}{\partial y}\right\|_{y=h} = 0, \quad i = CO_2, H_2O, Air$
Steam purging (steam)	1D	**At $z_{1/2}$:** • Pressure $P_{1/2} = P_1 - \frac{1}{2}\frac{\partial P}{\partial z_{1/2}}$ • Gas velocity $u_{1/2} = u_{inlet\ steam}$ • Temperature $\frac{\partial T}{\partial z_{1/2}} = 0$ • Concentration $\frac{\partial c_i}{\partial z_{1/2}} = 0, \quad i = CO_2, Air$ $\frac{\partial c_{H_2O}}{\partial z_{1/2}} = 1$	**At $z_{N+1/2}$:** • Pressure $\frac{\partial P}{\partial z_{N+1/2}} = 0$ • Gas velocity $\frac{\partial u}{\partial z_{N+1/2}} = 0$ • Temperature $\frac{\partial T}{\partial z_{N+1/2}} = 0$ • Concentration $\frac{\partial c_i}{\partial z_{N+1/2}} = 0, \quad i = CO_2, H_2O, Air$
Cooling (CL)	2D	**At $x = 0$ or $y = 0$** • Temperature $T(x = 0, y, t) = T_{wall}(t)$ $T(x, y = 0, t) = T_{wall}(t)$ • Concentration $\left.\frac{\partial p_i}{\partial x}\right\|_{x=0} = 0, \quad i = CO_2, H_2O, Air$ $\left.\frac{\partial p_i}{\partial y}\right\|_{y=0} = 0, \quad i = CO_2, H_2O, Air$	**At $x = \frac{b}{2}$ or $y = h$** • Temperature $\left.\frac{\partial T}{\partial x}\right\|_{x=\frac{b}{2}} = 0$ $\left.\frac{\partial T}{\partial y}\right\|_{y=h} = 0$ • Concentration $\left.\frac{\partial p_i}{\partial x}\right\|_{x=\frac{b}{2}} = 0, \quad i = CO_2, H_2O, Air$ $\left.\frac{\partial p_i}{\partial y}\right\|_{y=h} = 0, \quad i = CO_2, H_2O, Air$

Note S4: Steam-assisted vacuum-pressure temperature swing adsorption process description

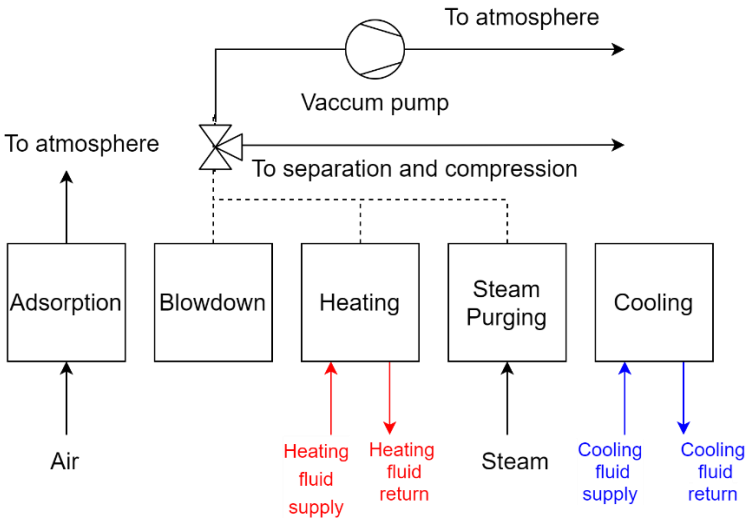

A systematic of SA-VTSA cycle.

The figure above shows the cyclic design for the SA-TVSA cycle, where all the boxes represent the same CO_2 collector. In the adsorption step, fans push the air through the collector, where CO_2 is adsorbed into the sorbent along with some H_2O. After the sorbent has reached the desired CO_2 saturation (97%), the collector is sealed and evacuated to vacuum (50 mbar) using a vacuum pump (i.e., blowdown step). This step is relatively fast, and the sorbent does not desorb a significant amount of CO_2 at this point, and thus mostly air is removed, which is vented back to the atmosphere. Removing the air from the contactor before heating the sorbent is important in case of utilizing amine-functionalised solid sorbents. This is because the amines in the sorbent can have critical degradation when exposed to oxygen at high temperature (i.e., oxidative degradation)[9-11]. For the desorption step, the sorbent is heated using a heating fluid at 100 °C using the heat transfer tubes, leading to the desorption of CO_2 and water, which are removed instantaneously due to the vacuum. After all points on the sorbent bed reach at least 95 °C, the heating fluid is stopped and the CO_2 collector is purged with steam (at steam gas velocity ($u_{inlet\ steam}$) of 0.01 m s^{-1}). The steam purging lowers the CO_2 partial pressure inside the collector, leading to an increase of the CO_2 working capacity. The steam purging step stops when the bed reach an average CO_2 loading of 0.1 mol CO_2 per kg sorbent. After the sorbent is regenerated, the bed is cooled down using a cooling fluid with a temperature above ambient temperature by 10 °C using the heat transfer tubes. The cooling step stops when all points on the sorbent are colder than 65 °C. Then, the collector is opened back to the atmosphere, and the cycle is repeated. The cooling step is important as the amine groups on the sorbent might get oxidized when the hot sorbent is contacted with oxygen in the air[9-11].

Supplementary Note S5: CO_2 compression modelling

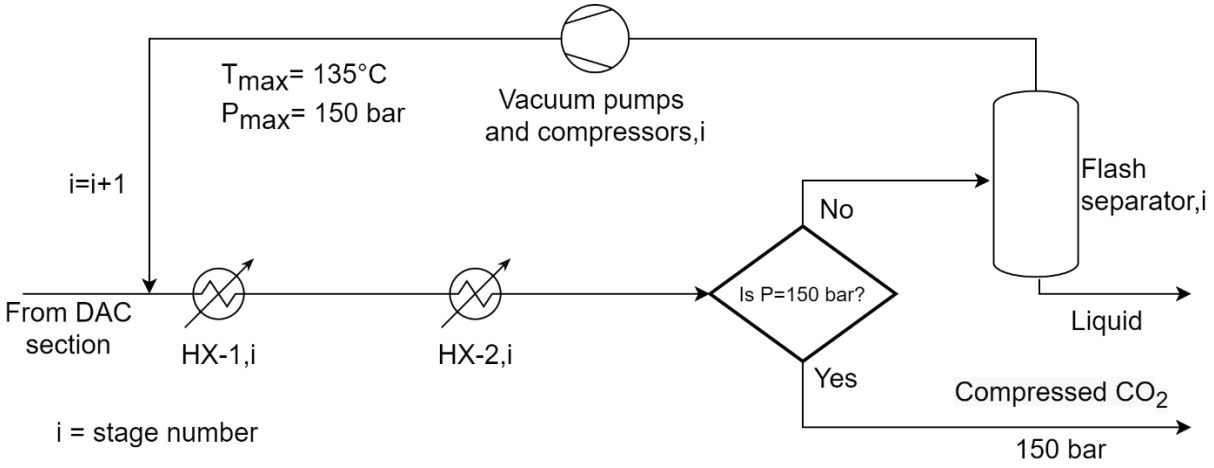

Process flow diagram of the CO_2 compression section.

The process section shown in the figure above is modelled using a combination of Aspen Plus V11 and MATLAB R2021a. Aspen Plus is used to provide fluid properties calculation where Lee Kesler Pokler (LKP) Equation of State (EoS) was selected as it was found to be suitable for the CO_2 and H_2O mixture[12]. MATLAB is used to automate the process synthesis as the section feed and operating parameters change due to changes in ambient conditions and feed conditions. In the automated process synthesis, HX-1 only recovers heat if the feed inlet temperature for HX-1 ($T_{inlet,HX-1}$) is above the heating fluid temperature $T_{heating}$ by the minimum approach temperature ΔT_{min}, which is 10°C in this work. HX-2 recovers the remaining heat and cools down the stream to ΔT_{min} above the ambient temperature T_{amb} such that CO_2 does not change phase to the liquid phase. When the feed stream contains mostly water, HX-2 recovers a substantial amount of low-temperature heat that is caused by condensing water, which cannot be recovered for preheating the steam water supply. Therefore, when accounting for the amount of heat that can be recovered from HX-2, if the inlet stream has a water mole fraction of more than 0.5, the heat is neglected and not recovered. The remaining amount of heat from HX-2 is recovered at 80% efficiency to account for any remaining water phase change.

The table below shows the algorithm used to set the parameters of the two heat exchangers where P_{sat,CO_2} and T_{sat,CO_2} are saturation vapor pressure and its temperature (i.e., boiling temperature). A higher temperature than CO_2 critical temperature and T_{sat,CO_2} are used as design margin.

An algorithm for the selection of operating parameter in the CO_2 compression section.

Equipment	Algorithm
HX-1	**if** $T_{inlet,HX-1,i} > T_{heating} + \Delta T_{min}$ $T_{outlet,HX-1,i} = T_{heating} + \Delta T_{min}$ **else** $T_{outlet,HX-1,i} = T_{inlet,HX-1}$
HX-2	**If** $P_{inlet,HX-2,i} = 150$ bar $T_{outlet,HX-2,i} = T_{amb} + \Delta T_{min}$ **elseIf** $P_{inlet,HX-2,i} > 74$ bar $T_{outlet,HX-2,i} = \max(T_{amb} + \Delta T_{min}, 35℃)$ **else** **if** $P_{inlet,HX-2,i} < P_{sat,CO_2}(T = T_{amb} + 5℃)$ $T_{outlet,HX-2,i} = T_{amb} + \Delta T_{min}$ **else** $T_{outlet,HX-2,i} = T_{sat,CO_2}(P_{in,HX-2}) + 5℃$

Note S6: Model validation

Climeworks reports the productivity of their 1st generation collector of 50 ktaCO_2 per collector[13] (ambient conditions were not reported for this collector productivity). Reported energy requirements[14] is based on daily averaged data from the two Climeworks plants (Hellisheidi, Iceland and Hinwil, Switzerland). It is not clear whether Climeworks uses steam purging in these plants (like the model in our paper), however, Climeworks do hold a patent for process configurations using steam purging after heating of the bed[15]. A comparison of the reported Climeworks data with the model results is summarised below in the table below. It is worth noting that energy requirements here are reported as separate thermal energy and electricity requirements. The thermal energy requirements include heat required for heating the bed (by the heating fluid) and steam generation, whereas electricity requirements include electricity needed for vacuum pumps compressors and fans. In the main paper, it is assumed that heat pumps that consume electricity are used to provide the thermal energy requirements needed to heat the bed (by the heating fluid) and generate steam. Thus, the reported electricity requirements in the main paper includes the heat pumps.

Comparison of the model results with Climeworks data.

	Our model		Climeworks data
	Hellisheidi DAC plant	**Hinwil DAC plant**	
Productivity (ktaCO_2 per collector)	56	55	50 (ref[13])
Thermal energy requirement (MWh_{th} per tCO_2)	3.42	3.46	3.31 (ref[14])
Electricity requirement (MWh_{el} per tCO_2)	0.26	0.27	0.70 (ref[14])
Fan electricity requirement (MWh_{el} per tCO_2)	0.06	0.06	0.08 (ref[3])

There is reasonable agreement between the model estimates of process productivity and thermal energy requirement with reported data by Climeworks for real-world units operating in two locations

(with temperatures below zero). However, for electricity requirements, there is a quite considerable deviation which was noticed before by Sabatino et al.[16]. The potential reasons for deviation may include sorbent type used and its weight per collector, process configuration, if steam purging or heat integration are used, and what is included in electricity requirements (e.g., building electricity, lights etc.) as well as vacuum pumps, compressors and fans efficiencies. Also, the electricity requirements for fans are compared to the data provided in the Climeworks patent[3]. Climeworks reported 0.08 MWh_{el} per tCO_2 at a fan efficiency of 70%, a pressure drop of 1 mbar through the adsorption bed, and a capture rate of 70%. Although we assume the same fan efficiency and target the same pressure drop, the calculated capture rate from the model is higher, which explains the slightly lower electricity requirements for fans of 0.06 MWh_{el} per tCO_2.

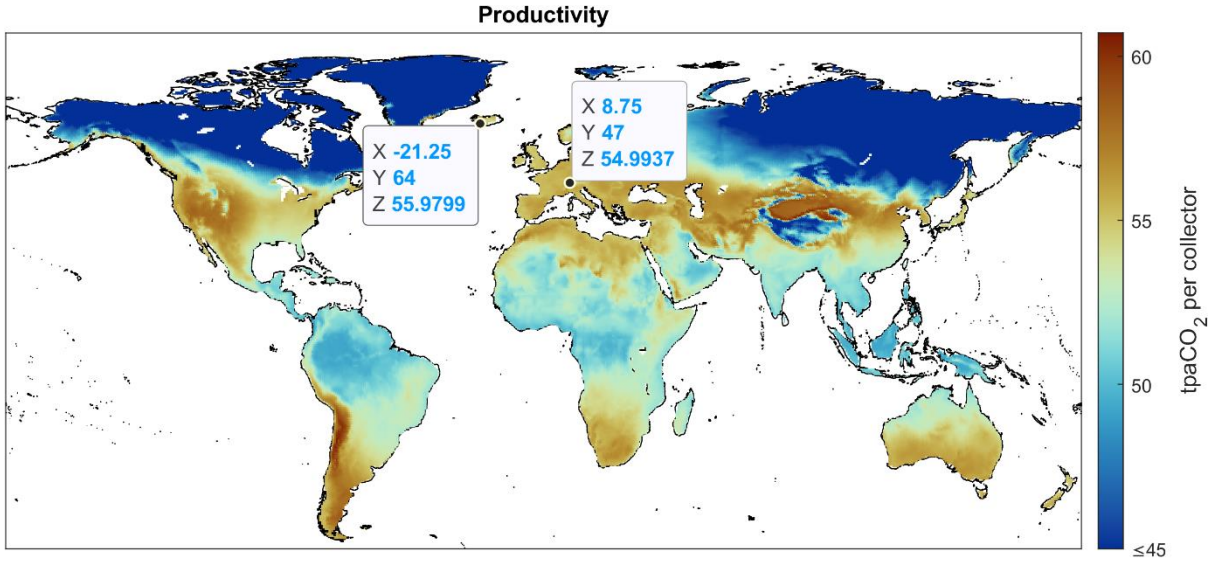

Collector productivity calculated from the model.

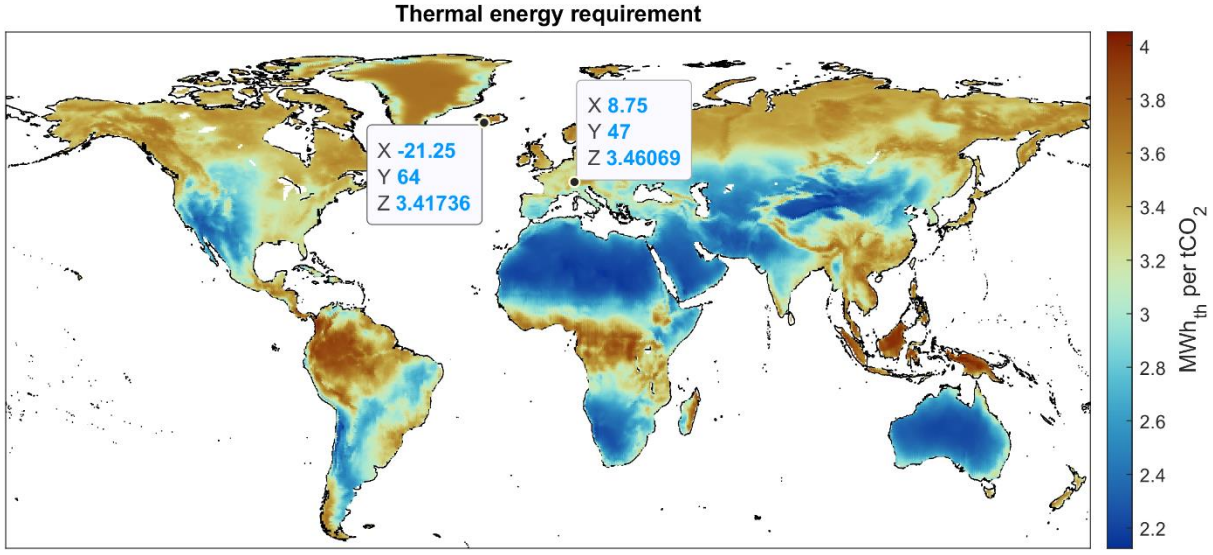

Thermal energy requirements include heat required for heating the bed (by the heating fluid) and steam calculated from the model.

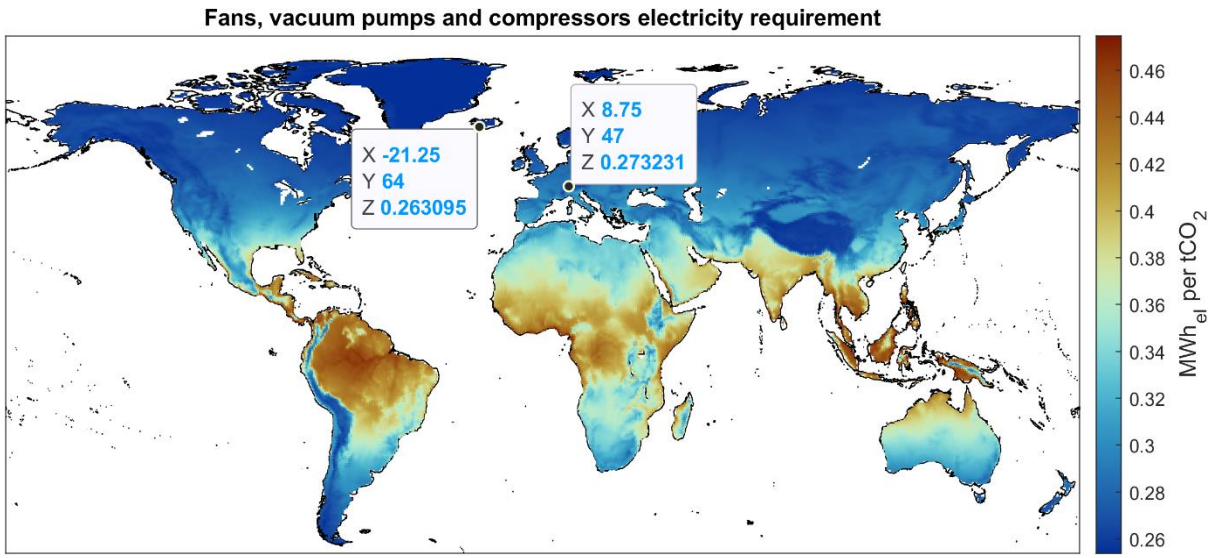

Electricity requirements include electricity required for fans, vacuum pumps, and compressors calculated from the model.

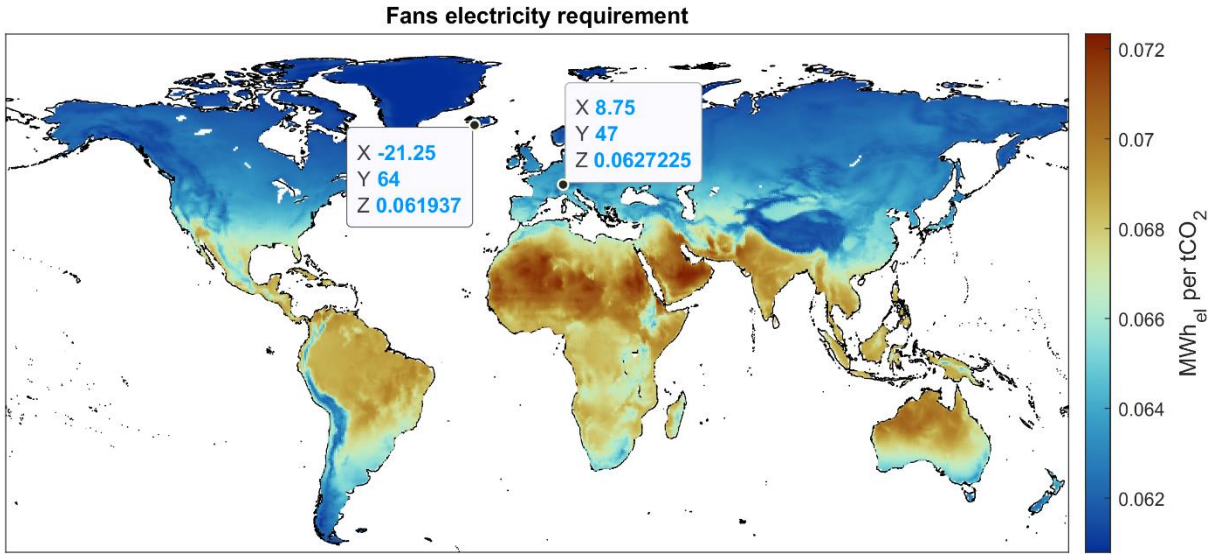

Electricity requirements for fans calculated from the model.

Note S7: standard deviation calculation

The standard deviation is calculated using MATLAB (2021a) function std. Since not all spatial nodes has the same area, weighted standard deviation is used where node DAC performance is weighted by the node area. The MATLAB std function uses the following relation:

$$S_w = \sqrt{\frac{\sum_{i=1}^{N} w_i |A_i - \mu_w|^2}{\sum_{i=1}^{N} w_i}}$$

$$\mu_w = \frac{\sum_{i=1}^{N} w_i A_i}{\sum_{i=1}^{N} w_i}$$

where

- A_i each value from the population,
- N size of the population,
- μ_w weighted mean,
- S_w weighted standard deviation,
- w weighting scheme.

References

1. Couper, J.R., Penney, W.R., Fair, J.R., and Walas, S.M. (2005). Chemical process equipment: selection and design (Gulf professional publishing).
2. Gebald, C., Wurzbacher, J.A., Borgschulte, A., Zimmermann, T., and Steinfeld, A. (2014). Single-Component and Binary CO_2 and H_2O Adsorption of Amine-Functionalized Cellulose. Environmental Science & Technology *48*, 2497-2504. 10.1021/es404430g.
3. Gebald, C., Piatkowski, N., Rüesch, T., and Wurzbacher, J.A. (2014) Low-pressure drop structure of particle adsorbent bed for adsorption gas separation process. patent 2014170184A1.
4. Terlouw, T., Treyer, K., Bauer, C., and Mazzotti, M. (2021). Life Cycle Assessment of Direct Air Carbon Capture and Storage with Low-Carbon Energy Sources. Environmental Science & Technology. 10.1021/acs.est.1c03263.
5. https://cars.lovetoknow.com/List_of_Car_Weights.
6. Vogtenhuber, H., Pernsteiner, D., and Hofmann, R. (2019). Experimental and Numerical Investigations on Heat Transfer of Bare Tubes in a Bubbling Fluidized Bed with Respect to Better Heat Integration in Temperature Swing Adsorption Systems. Energies *12*, 2646. 10.3390/en12142646.
7. Young, J., García-Díez, E., Garcia, S., and van der Spek, M. (2021). The impact of binary water–CO_2 isotherm models on the optimal performance of sorbent-based direct air capture processes. Energy & Environmental Science. 10.1039/D1EE01272J.
8. Wurzbacher, J.A., Gebald, C., Brunner, S., and Steinfeld, A. (2016). Heat and mass transfer of temperature–vacuum swing desorption for CO_2 capture from air. Chemical Engineering Journal *283*, 1329-1338. 10.1016/j.cej.2015.08.035.
9. Heydari-Gorji, A., and Sayari, A. (2012). Thermal, Oxidative, and CO_2-Induced Degradation of Supported Polyethylenimine Adsorbents. Industrial & Engineering Chemistry Research *51*, 6887-6894. 10.1021/ie3003446.
10. Bollini, P., Choi, S., Drese, J.H., and Jones, C.W. (2011). Oxidative Degradation of Aminosilica Adsorbents Relevant to Postcombustion CO_2 Capture. Energy & Fuels *25*, 2416-2425. 10.1021/ef200140z.
11. Stampi-Bombelli, V., van der Spek, M., and Mazzotti, M. (2020). Analysis of direct capture of CO_2 from ambient air via steam-assisted temperature–vacuum swing adsorption. Adsorption *26*, 1183-1197. 10.1007/s10450-020-00249-w.
12. White, C.W., and Weiland, N.T. (2018). Evaluation of Property Methods for Modeling Direct-Supercritical CO_2 Power Cycles. Journal of Engineering for Gas Turbines and Power *140*, 011701. 10.1115/1.4037665.
13. Viebahn, P., Scholz, A., and Zelt, O. (2019). The Potential Role of Direct Air Capture in the German Energy Research Program—Results of a Multi-Dimensional Analysis. Energies *12*, 3443.
14. Deutz, S., and Bardow, A. (2021). Life-cycle assessment of an industrial direct air capture process based on temperature–vacuum swing adsorption. Nature Energy *6*, 203-213. 10.1038/s41560-020-00771-9.
15. Gebald, C., Repond, N., and Wurzbacher, J.A. (2019) Steam assisted vacuum desorption process for carbon dioxide capture. patent 10279306B2.
16. Sabatino, F., Grimm, A., Gallucci, F., van Sint Annaland, M., Kramer, G.J., and Gazzani, M. (2021). A comparative energy and costs assessment and optimization for direct air capture technologies. Joule. 10.1016/j.joule.2021.05.023.